NASA TECHNICAL MEMORANDUM

NASA TM X-73666

NASA TM X-73666

STEADY-STATE UNBALANCE RESPONSE OF A THREE-DISK FLEXIBLE ROTOR ON FLEXIBLE, DAMPED SUPPORTS

by Robert E. Cunningham
Lewis Research Center
Cleveland, Ohio 44135

TECHNICAL PAPER to be presented at the
Vibrations Conference
sponsored by the American Society of Mechanical Engineers
Chicago, Illinois, September 26-29, 1977

STEADY-STATE UNBALANCE RESPONSE OF A THREE-DISK FLEXIBLE ROTOR ON FLEXIBLE, DAMPED SUPPORTS

by Robert E. Cunningham

National Aeronautics and Space Administration
Lewis Research Center
Cleveland, Ohio 44135

E-9091-1

ABSTRACT

Experimental data are presented for the unbalance response of a flexible, ball bearing supported rotor to speeds above the third lateral bending critical. Values of squeeze film damping coefficients obtained from measured data are compared to theoretical values obtained from short bearing approximation over a frequency range from 5000 to 31 000 cycles/min. Experimental response for an undamped rotor is compared to that of one having oil squeeze film dampers at the bearings. Unbalances applied varied from 0.62 to 15.1 gm-cm.

INTRODUCTION

The continuing search for improved performance of turboshaft machines is placing more emphasis on higher operating speeds (ref. 1). In addition to these higher rotating speeds there is a need to increase specific thrust ratios by reducing the overall weight of powerplants particularly for such applications as small helicopters, remotely piloted vehicles (RPV's) and small private and commercial aircraft (ref. 2).

Lower specific fuel consumption is an immediate goal of engine manufacturers. One area that is receiving the attention of engineering research is excessive leakage of air between compressor stages. To reduce such losses it is

STAR Category 07

necessary to reduce the seal clearances, particularly those at compressor blade tips. These reduced clearances, however, will also mean reductions in allowable amplitudes of rotor and frame vibrations.

Lighter powerplant structures, higher rotor operating speeds and smaller blade tip clearances places a great amount of emphasis on the dynamics of rotors, their bearings and the manner in which the bearings are mounted in the frame. The combination of lighter rotors and higher operating speeds can result in severe vibrations when operating through one or more lateral bending critical speeds.

Minimizing the amplitudes of rotor vibration at the lateral bending criticals means that techniques of balancing flexible rotors and shafts had to be greatly improved. This ultimately led to the development of new and improved balancing procedures, one of which is the influence coefficient method as described in reference 3.

Sometimes, however, it is not possible to achieve the desired low levels of vibration by balancing alone, particularly with the built up ball bearing supports and rotor assemblies which comprise the modern turbojet engine. Rotor assemblies, though balanced well initially, degrade with continued service time. Other means had to be developed to control both steady state and transient vibrations.

Coulomb (dry friction) and viscous oil shear types of mechanical dampers have been used for many years to control vibration amplitudes. Normally they were used in controlling torsional vibrations in all types of rotating machinery (ref. 4). Theinherent damping properties of hydrodynamic oil lubrication bearings were investigated by Hagg and Sankey in 1956 (ref. 5).

It is a well-known fact that the ball or roller bearings contain very little inherent damping. Such bearings are used almost exclusively in aircraft turbine engines. The availability of lubricating oil and the requirement of large amounts

of energy dissipation in a limited space were natural inducements to the ultimate development and use of an oil squeeze film dampter (ref. 6).

To properly design such a damper it is necessary to know something about the dynamic characteristics of the rotating system. Normally the machinery design engineer will have a number of computer programs available to him. Such programs can provide him with the flexible critical speeds and mode shapes of a particular rotor model in graphical output (ref. 7). The computer program referenced will also draw, to scale, a cross section of the rotor. It will also automatically plot critical speeds as a function of support stiffness. Unbalance response computer programs are also available that are capable of predicting the response of almost any type of rotor on flexible, damped supports. Damping coefficients can be an input to the program either as constants or as polynomial functions of rotor speed (ref. 8). The output of such programs, however, are only as accurate as the values of input such as support stiffness and damping

A number of analytical papers have been written which develop the equations for calculating squeeze film damping and stiffness coefficients; two such papers which use the short bearing approximation are references 9 and 10. It is then, one of the objectives of this paper to experimentally determine the oil squeeze film damping coefficients and to compare them with theory.

A second objective of this investigation is to examine the experimental response of a three-disk rotor to varying amounts of unbalance with and without squeeze film damping at the bearing supports. The results then would be compared to an unbalance response computer program similar to the one described in reference 8. This program however, was modified first, to consider only circular orbits and two, an iterative solution was added that includes support damping as a function of journal eccentricity ratio.

Unbalances tested varied from a low of 0.62 gm-cm to a high of 15.1 gm-cm. Three different types of unbalance distributions were investigated and these are:

Type I - Identical set screws were placed in the same radial plane in each of the three disks. The set screw in the center disk, however, was out of phase by 180^{o}.

Type II - Identical set screws were placed in the same radial plane in each of the two end disks only. The two screws were 180^{o} out of phase.

Type III - Identical set screws were placed in the same plane in all three disks.

Results were obtained over a speed range from 5000 to 31 000 cycles/min.

APPARATUS

Mechanical Features

Experimental data was obtained with the apparatus shown in the photographs and drawing of figures 1 through 5. The apparatus consists of a long slender shaft supported in ball bearings which are 48.3 cm apart. A single integral disk is located at midspan while removable disks of identical size, one at each end are located outside of the bearings (fig. 2). The rotor is 69.6 cm long and has a uniform diameter of 2.54 cm between bearings. The disks are 9.5 cm in diameter and contain threaded holes located every 10^{o}, on a bolt circle of 8.26 cm. Set screws can be placed in the holes as correction weights for balancing or to deliberately unbalance the rotor in a particular bending mode.

The rotor is supported in 204 series, radial ball bearings, one of which is shown in the photograph of figure 4. The outer races of these bearings are located in cylindrical steel housings, which also serve as the damper journal figures 3 and 4. Centering springs of 6061-T6 Aluminum shown in figure 4 have a yield stress of 296 MN/m^2 and when assembled locate the damper journal in the center of the damper bearing, this assembly can be seen in figure 3.

The squeeze film damper used in this investigation has an (L/D) ratio of 0.094 and is similar in design to the one described in reference 11, with the

following exceptions. No piston ring type of seals were used at the damper ends. The grooves, however, were retained (see fig. 3) Also given in figure 3 are all pertinent damper dimensions. The piston ring seals were eliminated because they introduced a tare damping and stiffness that could not be readily quantified. Eliminating the end seals, however necessitated a reduction in damper radial clearance from 127 μm to a nominal clearance of 64 μm in order to keep damper oil flows within the pumping capacity of the oil supply system. The lubricating and damping oil was a typical turbojet engine oil. Type II ester meeting the specifications of MIL-L-23699A.

The flow of oil to each damper could be controlled independently with needle valves located in each of the supply lines. This flow, however, was held constant at 5.5×10^{-4} m^3/min in all the tests conducted. Temperature of the oil could be maintained within 2° C over the elapsed time of a typical test run.

The test rotor was driven by a 10.16-cm diameter air turbine having a maximum operating speed of 60 000 rpm. The turbine was connected to the test rotor by means of a 0.95-cm diameter quill shaft and a spline coupling (see figs. 1 and 2).

Instrumentation

Deflections of the test rotor from a neutral axis were sensed by noncontacting, eddy current probes. These probes were located in mutually perpendicular axes at each of the three disks. Distance sensor pairs were also cemented into the damper bearings flush with its surface to measure damper journal motion.

Transducers used for measuring the forces transmitted through the damper oil squeeze film are quartz crystal, piezoelectric load washers. The load capacity is 35.6×10^3 N with a stiffness of 175×10^8 N/m while having a resonant frequency of 50 000 hertz. Linearity over the load range was 1 percent, these transducers can be seen in figure 5.

DISCUSSION OF RESULTS

The results of this investigation are presented in figures 6 through 14 and in table I, and are discussed under two separate headings. The first examines the response of a three-disk rotor to various magnitudes of unbalance. Three different types of unbalance distributions were tested, these were described in the INTRODUCTION, they are also shown schematically in table I. The second part of the discussion will compare experimentally determined values of damping coefficients with those predicted by theory, and for unbalances ranging from 0.62 to 15.1 gm-cm and rotor frequencies to 31 000 cycles/min. These results are plotted in figures 13 and 14

Unbalance Response

Before any tests were conducted it was necessary to determine the undamped critical speeds and mode shapes. These were determined from the computer program of reference 7 and are plotted in figure 7 for a spring stiffness of 2.36 MN/m. The deflections are only relative but do indicate that oil squeeze film dampers placed at the bearing supports should be effective when operating through all four bending critical speeds.

Before any deliberate unbalance distributions could be tried, the rotor had to be dynamically balanced. First attempts to balance the rotor without any squeeze film damping at the supports indicated a high degree of sensitivity of a ball bearing supported rotor to very small amounts of unbalance. Using a combination of the influence coefficient method, reference 3 and a single plane, vector plot, resulted in a well-balanced rotor capable of negotiating all critical speeds below 31 000 cycles/min with no more than a 10-μm or less, peak-to-peak amplitude.

Figures 7, 8, and 9 compare the undamped rotor response with the response when oil squeeze film dampers are activated. The plotted traces in figures 7, 8,

and 9 are that of the filtered signal generated by either proximity distance sensors or piezoelectric crystal force transducers. The 10-hertz bandwidth filter tracks on the rotor frequency and, therefore, the trace is that of the rotor synchronous response only. Comparisons between undamped versus damped response are for very small unbalances of 0.62 and 0.93 gm-cm because operating the rotor without any external damping at the bearings could have resulted in damaging the rotor and stationary seals if larger unbalances had been tested.

The amplitude versus frequency plot of figure 7 was produced by an inline, alternating phase distribution of weights in the three disks. The unbalance weights in the end disks are 180^{o} out of phase with the weight in the center disk as depicted by the inset drawing. The total unbalance distributed over three disks is 0.93 gm-cm. The three set screws used as unbalance weights were carefully matched in weight and did not vary more than 4 mg.

The amplitudes of motion plotted in figure 7 are of the number 3 disk. A maximum peak-to-peak amplitude of approximately 100 μm, above machining runout, was recorded for the rotor operating with no externally applied damping.

The undamped rotor exhibits three distinct amplitude buildups at frequencies close to the ones predicted by the critical speeds program of reference 7. The maximum undamped resonant amplitude occurs at about 9500 cycles/min. The type of unbalance distribution used in these trials would normally excite the first and third bending critical speeds as can be seen from the mode shapes of figure 6. Therefore, it is reasonable to expect larger amplitudes at resonant frequencies corresponding to those modes. It should be pointed out that even though no external squeeze-film damping was present in this trial, it is obvious that some amount of damping is present in the oil lubricated ball bearings. The maximum amplitude predicted by an unbalance response program, for an assumed ball bearing damping of 3500 N·sec/m is 381 μm at 7500 cycles/min.

Turning our attention to the lower portion of figure 7, where oil squeeze film dampers were activated, shows one distinct buildup in amplitude instead of three. The mode shape for this damped critical occurring at 10 000 cycles/min was determined to be similar to the one at the third bending critical shown in figure 6. The maximum peak-to-peak amplitude, when the dampers were activated, was approximatelv 90 μm. The peak-to-peak amplitude at the center disk was 216 μm, not a significant improvement for this unbalance distribution. The unbalance response program predicted a maximum peak-to-peak amplitude at the center disk of approximately 85 μm at 9600 cycles/min and about 45 μm for the number 3 disk. The agreement between experiment and theory for this unbalance distribution is not very good. Because of the large rotor excursion exhibited for unbalances of 0.93 and 1.67 gm-cm tests at greater unbalances were not attempted for fear of damaging rig components such as the labyrinth seals located at the bearing supports.

The number 3 disk wants to move out at amplitudes greater than indicated in the undamped test of figure 7. However, the damper journal can move out only as far as the clearance in the damper bearing will permit, and this is approximately 127 μm total movement. This may account for the jagged appearance of the trace at the second and third criticals. With the activation of the dampers the trace smooths out; again the theoretical prediction of the maximum amplitude of 44 μm is low.

Low speed measurements made along the shaft from bearing to bearing indicated a bow or warping of the shaft was present in the "as received" condition. The amount of warp or bow measured was approximately 10 to 13 μm maximum at either side of the center disk. This shaft runout can be seen at the low speeds in all of the plots. Inadvertently, the inline unbalance distribution was placed in a plane only 40° away from the plane of the residual warp. This then could account for the shaft having a strong preference to bend a greater amount in this plane over any other.

The rotor response shown in figure 8 is for an inline, alternating phase distribution, for two disks only; the center disk did not have an unbalance weight (see inset figure). This type of unbalance distribution should have excited the second mode shape (see fig. 6). The undamped response, however, is similar to the previous response for three disk inline, alternating phase. Activating the oil film dampers resulted in a significant reduction in the resonant amplitude. An amplitude of approximately 12 μm over the machining runout was recorded at 9700 cycles/min while the unbalance response program predicted a peak-to-peak amplitude of only 1.3 μm at 10 000 rpm.

The unbalance distribution used to generate the experimental response shown in figure 9 for the number 3 disk, is an inline, inphase distribution using all three disks, Type III (see inset drawing). The oil squeeze film dampers cause a reduction in the peak-to-peak amplitude of over 80 percent at the end disk and approximately 70 percent for the center disk. The damped response for inline, inphase unbalance distribution applied to the test rotor correlated well with the predicted response at very small unbalances of 0.93 gm-cm as shown in figure 9.

It was decided to examine the response for much greater magnitudes of unbalance. In figures 10(a) through (d) comparisons are made between the actual and theoretical damped rotor response. It is quite apparent in figure 10(a), which is the peak-to-peak amplitude of the center disk, that squeeze film dampers located at the bearings of a long slender rotor are going to have little effect on attenuating midspan excursions. The agreement between the actual response and the predicted is quite good for both the amplitude and the frequency at which resonance occurs.

The theoretical response program will predict, with considerable accuracy, the amplitudes, phase angles, and forces transmitted providing the input data, such as support flexibility and damping are accurate. In this case the matchup

at the center disk is close. Stiffnesses of the centering springs were carefully measured and this value (2.36 MN/m) entered in the program as input. Damping coefficients were calculated from theory and for this case agreed quite well with measured values at least at the resonant frequency. Damping values of 6300 N·sec/m are shown on the plots and were calculated for a concentrically positioned damper journal ($\eta = 0$).

It should be noted here that the recorded amplitudes of motion and transmitted forces were in the vertical or y direction. Response was also measured in the X-direction and appeared similar to Y measurements. The value of radial clearance used in calculating the damping for the theoretical unbalance response was 63.5 μm, which was also the measured assembled clearance.

Considerable disagreement is apparent between the measured amplitudes of motion and the theoretical for both the end disk and the damper journal, as shown in figures 10(b) and (c), respectively. The thereotical response is much greater than the measured response at frequencies above 10 000 cycles/min. It is not exactly clear as to why such disagreement exists at the higher unbalances of 10.6 and 15.1 gm-cm. It is apparent that the rotor end and damper journal opposite the turbine appear to deflect much less than predicted. The reason for this may be attributed to the non-cylindrical shape of the damper bearing (see fig. 5). The walls of the bearing in those locations where distance probes are mounted, are reduced in thickness. It is possible that flexing of this member was taking place, particularly with the higher rotating unbalance loads and therefore the absolute damper journal motions measured were less than if the damper bearing were perfectly rigid. The transmitted force also would be less in the actual system (see fig. 10(d)) since it is the vector sum of the elastic and damping film forces, both of which in turn are functions of the displacement.

The photographs of figure 11(a) are of the damper journal orbital motion. The pictures on the left are for an undamped system, damper oil supply off.

Those pictures on the right are for identical conditions of unbalance, magnitude, and frequency except that now oil is being supplied to the dampers. It should be pointed out that these pictures are of the unfiltered signals and, therefore, Lissajous patterns of orbital motion are generated which can be nonsynchronous as well as synchronous. The scale shown to the side of each picture should be noted carefully since it is not the same in each picture.

The large orbit at 9020 cycles/min is of the undamped journal motion. This is a synchronous critical with a peak-to-peak amplitude of 96.4 μm. The amplitude, frequency traces of figure 11(b) are for filtered signals made at the same time as the photographs. The first picture was snapped while the rotor was approaching the second critical speed of 9600 rpm. The undamped trace of figure 11(b) shows only resonances which are synchronous. Some of the multiple harmonics that occur in a lightly damped ball bearing supported rotor can have large amplitudes that can be quite destructive. These motions would not be seen at all if only the filtered trace were being observed. The Lissajous patterns at 25 710 rpm, for the undamped rotor, figure 11(a) has one inward loop; this signifies a multiple harmonic having a frequency twice that of the rotor speed. This orbit is a result of the gravity vector of a horizontally supported rotor superimposed on the unbalance whirl vector (ref. 12). The noteworthy point to be made concerning the pictures (fig. 11(a)) is that oil-squeeze-film damping is very effective in attenuating the motions of both synchronous and nonsynchronous whirl.

Oil Squeeze Film Damping

Presented in figures 12 through 14 are values of oil squeeze film damping coefficients, the force transmitted through the oil film and dynamic eccentricity ratio (ϵ) all plotted as functions of rotor frequency. Eccentricity ratio, as defined here, is the average of peak-to-peak journal displacements in the X and Y

coordinate directions planes divided by the radial clearance in the damper. Table I contains a summary of average damping coefficients at different magnitudes of unbalance and types of unbalance distributions.

The experimental values obtained in this investigation are averages calculated from amplitudes, forces and phase angles measured in both X and Y coordinate direction planes Damper journal distance probes had to be located in planes 45° from the force transducers (see fig. 5). To obtain the correct phase angles φ, the recorded angles had to be adjusted by 45°. This probably resulted in a slight error in calculating the damping coefficients, but due to the near circularity of orbits (see fig. 11(a)) the error introduced was not large.

Values of damping coefficient were obtained by measuring the force transmitted (F_{TR}) through the oil film to the damper bearing, the displacement of the damper journal (e), the angle φ by which the displacement lags the exciting force (acts 180° from transmitted force) and the rotor frequency, ω.

The derivation of the equations used in the data reduction is given in the appendix and the derived expressions are as follows:

Damping coefficient

$$B_{x,y} = \frac{\left(F_0\right)_{x,y} \sin \varphi_{x,y}}{e_{x,y}\omega}$$

Stiffness coefficient

$$K_{x,y} = \frac{\left(F_0\right)_{x,y} \cos \varphi_{x,y}}{e_{x,y}}$$

F_0 is the amplitude of the transmitted force. Values of stiffness coefficient are not presented in this report. The values, as would be calculated

from the above expression depend on the cosine of the measured phase angles. The accuracy of the measured angle near 90° is $\pm 1^{\circ}$ (approx.) This error is not serious when the sine of the angle is taken, since the sine does not vary significantly for a 2° change when near 90°. However, the cosine does vary significantly for a change of 2° and, consequently, there is a large error introduced when calculating values of the oil film stiffness coefficient.

Theoretical damping coefficients plotted in figures 12 through 14 were calculated from the following equation:

$$B = \frac{\pi \mu R L^3}{C_R^3 \left(1 - \eta^2\right)^{3/2}}$$

where μ is oil viscosity; R is journal radius, L is journal land length, C_R is radial clearance, $C_d/2$; and η is the conventional journal eccentricity ratio e/C_R defined as a static deflection e_0 divided by the radial clearance C_R; η is zero for the theoretical damping coefficients calculated in figures 12 through 14. The eccentricity ratio ϵ (dynamic eccentricity ratio) plotted in these same figures, is defined as the radius of the orbit e, divided by the radial clearance, C_R. For $\eta = 0$ and 180° film the theoretical damping coefficients appears as a straight line in figures 12 through 14.

The above equation is derived from the Reynolds lubrication equation for oil and squeeze film subjected to a periodic dynamic loading. It is for the case of a 180° film extent (cavitated bearing) using short bearing theory (ref. 10).

Results plotted in figures 12(a) and (b) are for an inline, alternating phase unbalance distribution, with a total unbalance of 0.93 and 1.67 gm-cm, respectively. Average values for the experimental damping coefficient (see table I) were 6750 and 6531 N·sec/m for unbalances of 0.93 and 1.67 gm-cm as compared to values of 6492 and 6213 N·sec/m for the theoretical, 180° film extent. The average

values calculated over the frequency range are slightly higher than the theoretical, however, for the most part, the agreement can be considered as good. The agreement between experiment and theory for the transmitted force and eccentricity ratio is not very good however, considerable deviation is apparent, particularly at rotor speeds above 16 000 cycles/min. The experimental data indicates that some sort of resonance is being approached between 28 000 and 30 000 cycles/min.

The unbalance response program predicts a resonance of approximately 33 000 cycles/min and therefore does not reflect any significant buildup in amplitude at these frequencies. This same increase in amplitude at 28 000 cycles/min is also apparent in the damped trace of figure 7.

The results plotted in figures 13(a) and (b) are for inline, alternating phase unbalance distribution with the two end disks only, and designated unbalance Type II. The experimental values of damping coefficients have somewhat more scatter than the previous data, however, the values do not deviate significantly from the theoretical 180° cavitated film, as predicted by short bearing theory. Experimental values of damping coefficient appear to deviate from theory most at rotor frequencies near the critical which is approximately 9600 cycles/min. Phase angles, when approaching the critical frequency, are changing very rapidly and therefore, are subject to greater error than those measured at frequencies greater than the critical frequency. Also, rotor orbits at these frequencies, instead of being circular, are all elliptical.

Agreement between theory and experiment for the transmitted force and the eccentricity ratio are quite good throughout most of the frequency range. Experimental values tend to increase at a faster rate at higher rotor speeds as in the previous plots.

In figures 14(a) through (d) the unbalance distribution used was Type III an inline, inphase distribution. Magnitudes of total unbalance tested varied from

0.93 to 15.1 gm-cm, however, only values of 2.25 to 15.1 gm-cm are plotted. The average experimental values listed in table I vary from 6.8 percent below to 9.2 percent above the predicted values. The trend, however, indicates experimentally determined damping coefficients, for these series of tests, are in good agreement with values calculated from short bearing theory and for a 180^{o}, cavitated film. Experiments also indicate that damping coefficients are not a strong function of the dynamic eccentricity ratio ϵ but in general, remain fairly constant. Similar results are presented in reference 13, that is, squeeze film damping coefficients, although greater in magnitude than 180^{o} film theory remained fairly constant at dynamic eccentricity ratios varying from 0.03 up to 0.4 for an end fed damper with a length to diameter ratio, L/D = 0.34.

The data plotted in figures 14(b), (c), and (d) are for total unbalances of 4.97, 10.6, and 15.5 gm-cm. It was thought that the resulting higher dynamic eccentricity ratios would result in slightly higher values of damping coefficients. This did not occur in fact, an opposite trend was observed in that damping coefficient actually decreased. It was also observed that a hydrodynamic instability was induced. This is referred to in the literature (refs. 14 and 15) as a bi-stable operation. Briefly, this is where the damper journal can operate in a stable condition at either of two eccentricity ratios. The region of frequency where this instability occurred is shown in figures 14(c) and (d). The rapid increase in journal amplitude is also shown at approximately 25 000 rpm in figure 10(c). A region is indicated since the bi-stable phenomenon noted did not always occur at exactly the same frequency in subsequent trials. It is not the purpose of this investigation to examine nonsteady state behavior such as occurred, other than to note its effect in the reduction of the damping coefficient. An increase in the oil flow to the damper was also noted to occur at frequencies approaching the bi-stable region. It is postulated that the damper at this juncture became starved with an accompanying rupture of the oil film. This would then account for the decrease in damping coefficients above the instability region.

SUMMARY OF RESULTS

Experimentally determined values of squeeze film damping coefficients were in good agreement with theoretical values calculated from equations derived by the short bearing approximation for a 180° film extent, and a concentrically positioned damper journal ($\eta = 0$). Values remained fairly constant at rotor frequencies to 31 000 cycles/min.

Central feed groove type of oil squeeze film dampers, located at the bearings were most effective in reducing amplitudes of motion at the rotor ends. They were, however, less effective in attenuating amplitudes of motion at the rotor center. A reduction in amplitude of over 80 percent was observed for an unbalance of 0.93 gm-cm distributed inline, inphase over three disks.

When oil squeeze film dampers were activated for an inline, alternating phase type of unbalance distribution, three distinct undamped resonant amplitudes were reduced to only one. The mode shape for this one corresponds to the third bending critical.

The oil squeeze film dampers were effective in reducing the amplitudes of motion for non-synchronous whirl as well as synchronous.

An unbalance response computer program was found to be reasonably accurate in predicting the response of the three-disk experimental rotor used in this investigation. The discrepancies that did occur apparently were due to the presence of a residual bend in the rotor having a shape similar to that which occurs at the first critical speed. The placement of weights in a line and near the plane of residual bend induced greater bending than would probably have occurred with a straight shaft. Conversely, locating the center weight 180° from the two end disks resulted in the rotor not bending as much as predicted by theory.

Unbalances of 10.6 and 15.1 gm-cm arranged inline, and inphase in all three disks produced an instability in the rotor referred to as bistable operation.

Values of damping coefficient were reduced significantly at frequencies greater than the onset frequency. Increased flow rates of damper oil were observed that might have resulted from the higher damper journal eccentricities and increased hydrodynamic pumping.

Resonant amplitudes were observed with the undamped rotor which occurred at frequencies slightly greater than those predicted by a critical speeds, mode shape program.

REFERENCES

1. Vance, J. M. and Royal, A. C., "High-Speed Rotor Dynamics - An Assessment of Current Technology for Small Turboshaft Engines," Journal of Aircraft, Vol. 12, 1975, pp. 295-305.

2. Hamburg, G. W., et al., "Design and Development of Low Cost, Self-Contained Bearing Lubrication Systems for Turbine Engines," Journal of Aircraft, Vol. 12, 1975, pp. 253-259.

3. Tessarzik, J. M.: Badgley, R. H.; and Anderson, W. J., "Flexible Rotor Balancing by the Exact Point-Speed Influence Coefficient Method," Journal of Engineering for Industry, Vol. 94, 1972, pp. 148-158.

4. Den Hartog, J. P., Mechanical Vibrations, 4th ed., McGraw-Hill, New York, 1956, p. 210.

5. Hagg, A. C. and Sankey, G. O., "Some Dynamic Properties of Oil-Film Journal Bearings with Reference to the Unbalance Vibrations of Rotors," Journal of Applied Mechanics, Vol. 23, 1956, pp. 302-306.

6. Brown, P. F., "Bearings and Dampers for Advanced Jet Engines," Paper 700318, SAE, 1970.

7. Trivisonno, R. J., "Fortran IV Computer Program for Calculating Critical Speeds of Rotating Shafts," NASA TN D-7385, 1973.

8. Lund, J. W., "Rotor Bearing Dynamics Design Technology. Part V: Computer Program Manual for Rotor Response and Stability," Air Force Aero-Propulsion Laboratories Report AFAPC-TR-65-45-Pt-V, May 1965.

9. Mohan, S. and Hahn, E. J., "Design of Squeeze Film Damper Supports for Rigid Rotors," Journal of Engineering for Industry, Vol. 96, 1974, pp. 976-982.

10. Barrett, L. E. and Gunter, E. J., "Steady-State and Transient Analysis of a Squeeze Film Damper Bearing for Rotor Stability," NASA CR-2548, 1975.

11. Cunningham, R. E., Fleming, D. P., and Gunter, E. J. Jr., Design of a Squeeze-Film Damper for a Multi-Mass Flexible Rotor," Journal of Engineering for Industry, Vol. 97, 1975, pp. 1383-1389.

12. Dimentberg, F. M., Flexural Vibrations of Rotating Shafts, Butterworths, London, 1961, p. 191.

13. Tonneson, J., "Experimental Parametric Study of a Squeeze Film Bearing," Journal of Lubrication Technology, Vol. 98, 1976, pp. 206-213.

14. White, D. C., Conference on Vibrations in Rotating Systems, Proceedings, Inst. Mech. Eng., London, 1972, p. 213.

15. Semandiri, S. and Hahn, E. J., "Effect of Pressurization on the Vibration Isolation Capability of Squeeze Film Bearings," Journal of Engineering for Industry, Vol. 98, 1976, pp. 109-117.

APPENDIX - DERIVATION OF DATA REDUCTION EQUATIONS

The force transmitted through the oil film to the damper bearing, and measured by the force transducers, is equal to the sum of the elastic force, the dissipative or damping force, and the oil film inertia force.

Transmitted Force = Elastic Force + Damping Force + Inertia Force

Because the volume of oil in the squeeze film is so small the inertia force can be neglected and:

$$\left(F_{TR}\right)_{x,y} = K_{x,y}(x,y) + B_{x,y}\frac{d(x,y)}{dt} \tag{1}$$

It is assumed that the journal precesses about the bearing center in an elliptical orbit and the motion is harmonic:

$$x = e_x \cos \omega t; \qquad y = e_y \sin \omega t \tag{2}$$

$$\frac{dx}{dt} = -e_x \omega \sin \omega t; \qquad \frac{dy}{dt} = e_y \omega \cos \omega t \tag{3}$$

Let $\left(F_0\right)_{x,y}$ be the amplitudes of the transmitted force in the X and y directions, respectively; then:

$$F_x = \left(F_0\right)_x \cos(\omega t + \varphi_x); \qquad F_y = \left(F_0\right)_y \sin(\omega t + \varphi_y) \tag{4}$$

Substituting equations (2), (3), and (4), in (1) we obtain:

$$F_x = K_x e_x \cos \omega t - B_x e_x \omega \sin \omega t = \left(F_0\right)_x \cos(\omega t + \varphi_x) \tag{5}$$

and

$$F_y = K_y e_y \sin \omega t + B_y e_y \omega \cos \omega t = \left(F_0\right)_y \sin(\omega t + \varphi_y) \tag{6}$$

where φ_x and φ_y are the angles by which the displacement lags the exciting force, see sketch below:

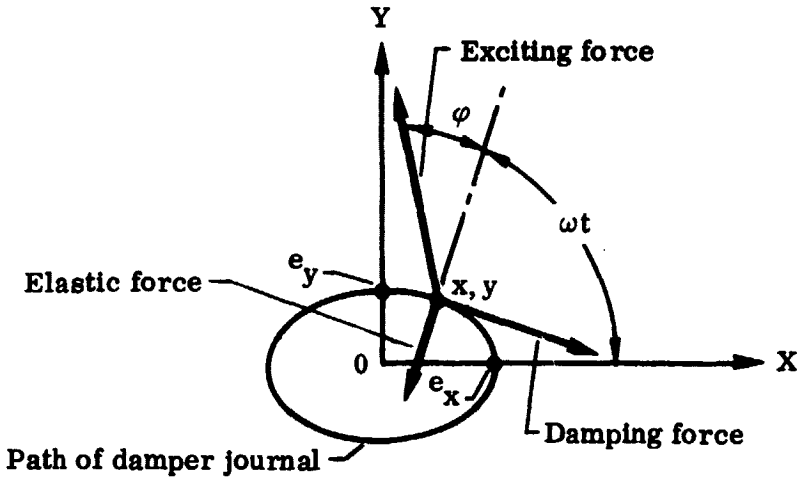

for $y = 0$; $x = e_x$; $\omega t = 0$ and solving for the stiffness and damping coefficients

$$K_x e_x(1) - B_x e_x \omega(0) = \left(F_0\right)_x \cdot \cos(0 + \varphi_x)$$

$$K_x = \frac{\left(F_0\right)_x \cos \varphi_x}{e_x} \tag{7}$$

$$K_y e_y(0) + B_y e_y \omega(1) = F_{0_y} \sin(0 + \varphi_y)$$

$$B_y = \frac{\left(F_0\right)_y \sin \varphi_y}{e_y \omega} \tag{8}$$

for $X = 0$; $y = e_y$; $\omega t = \pi/2$ and again solving for the stiffness and damping coefficients

$$K_x e_x(0) - B_x e_x \omega(1) \doteq \left(F_0\right)_x \cos(\pi/s + \varphi_x)$$

$$B_x = \frac{\left(F_0\right)_x \sin \varphi_x}{e_x \omega} \tag{9}$$

$$K(e_y)(1) + B e_y \omega(0) = \left(F_0\right)_y \cos \varphi_y$$

$$K_y = \frac{\left(F_0\right)_y \cos \varphi_y}{e_y} \tag{10}$$

The transmitted forces in the X-Y coordinate planes are measured along with the journal displacements in orthogonal planes. The rotor frequency, ω is also measured and knowing these values, the dynamic film coefficients in the X-Y planes can be solved for.

TABLE I. - SUMMARY OF EXPERIMENTAL AND THEORETICAL DAMPING COEFFICIENTS

AT VARYING TYPES AND MAGNITUDES OF UNBALANCE

Damper geometry

r = 3.95 cm

L = 0.74 cm

C_R = 63.5 μm

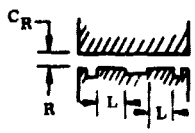

Type of oil: Type II ester meeting specifications of MIL-L-23699-A

Viscosity at 38° C = 0.033 (N-sec)/m^2

Oil flow = 5.15×10^{-4} M^3/min

Supply press = 19.29×10^4 N/m^2

Type of unbalance distribution	Magnitude of total unbalance (gm-cm)	Frequency range (cycles/min)	Average damping coefficients (N-sec/m) for (η = 0)	
			Experimental	Theoretical
Type I - Inline, alternating phase, 3 disks 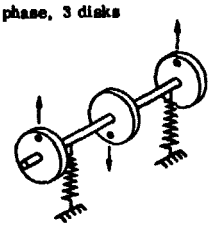	0.93	11 000 - 31 000	6740	6492
	1.67	10 000 - 31 000	6531	6213
Type II - Inline, alternating phase, 2 end disks 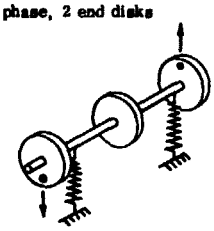	0.62	7 000 - 26 000	6029	6213
	1.11	7 000 - 28 000	6265	5408
	1.5	7 000 - 28 000	6843	6212
	3.3	6 000 - 29 000	5416	5880
Type III - Inline, same phase, 3 disks 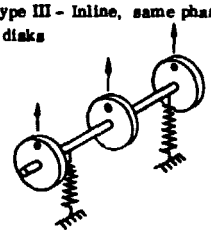	0.93	6 000 - 22 000	5478	5758
	1.67	7 000 - 24 000	5708	5425
	2.25	6 000 - 23 000	5926	5425
	4.97	5 000 - 22 000	5880	5425
	10.6	6 000 - 30 000	5289	6108
	15.1	5 000 - 25 000	6375	6843

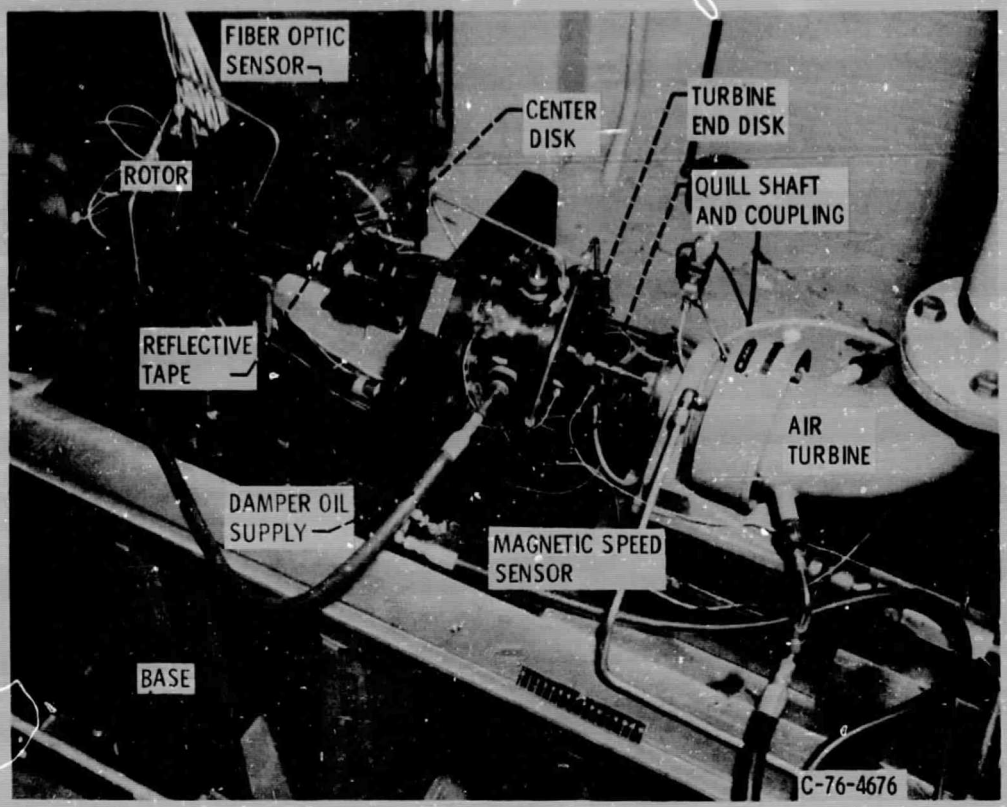

Figure 1. - Test apparatus used in experiments on steady-state unbalance response.

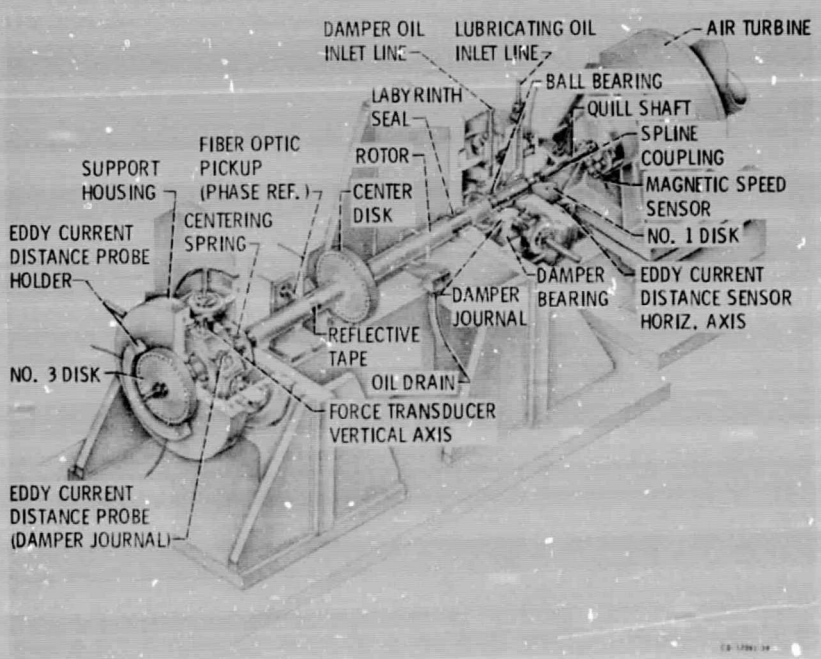

Figure 2. - Schematic of test apparatus used in experiments on steady state unbalance response.

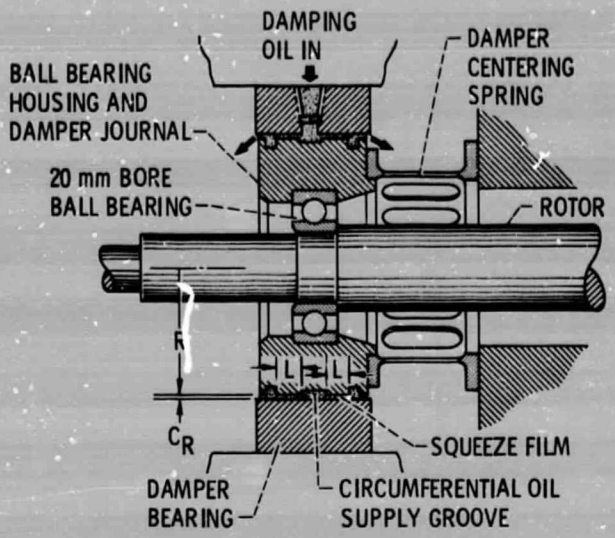

R, DAMPER JOURNAL RADIUS, 3.96 cm
L, DAMPER JOURNAL LAND LENGTH, 0.74 cm
C_R, DAMPER RADIAL CLEARANCE, 63.5 cm

Figure 3. - Schematic of oil squeeze film damper used in experiments for the steady-state response of a 3 disk rotor.

E-701

Figure 4. - Components of flexible damped support.

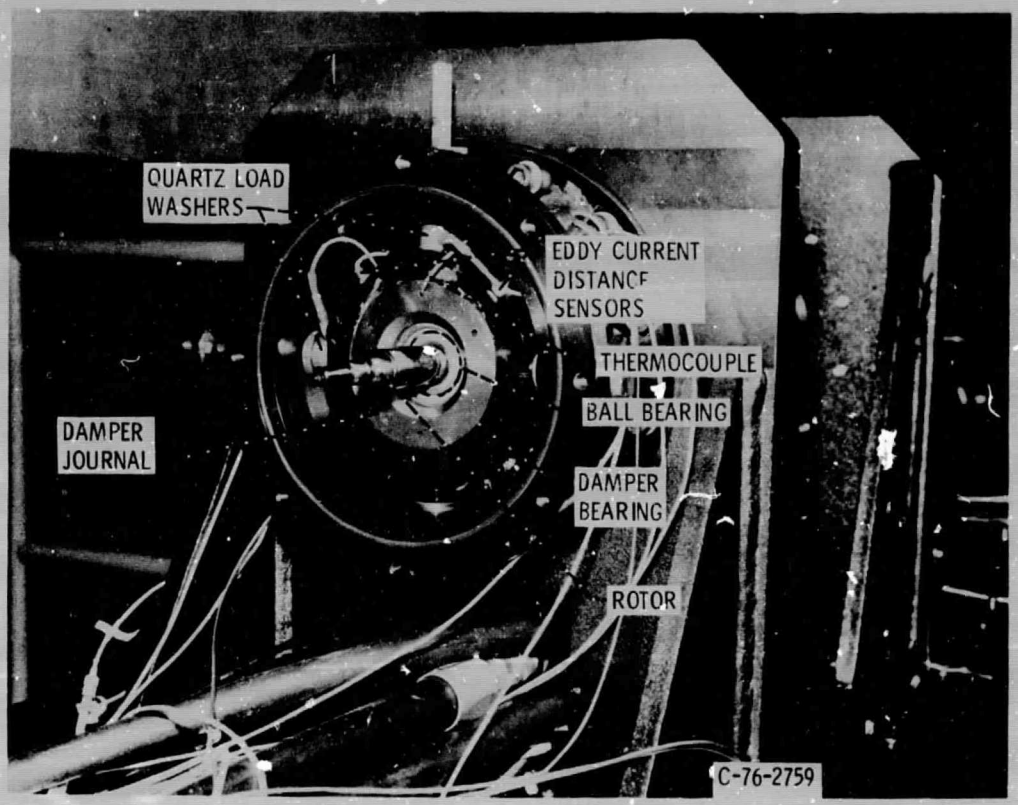

Figure 5. - End view of test apparatus showing No. 2 ball bearing and oil squeeze film damper.

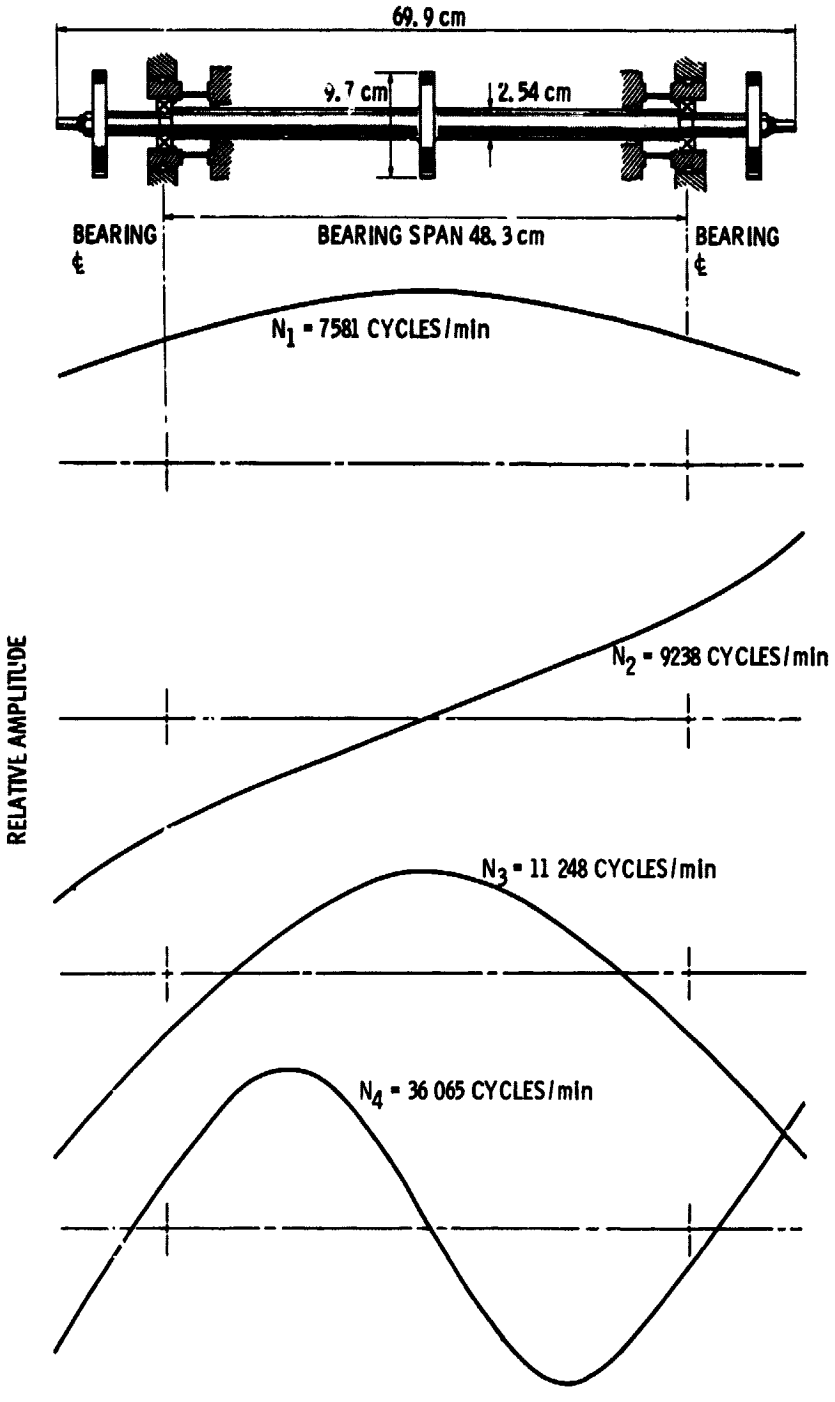

Figure 6. - Undamped critical speeds and mode shapes, centering spring stiffness, $K = 23.63 \times 10^5$ N/m.

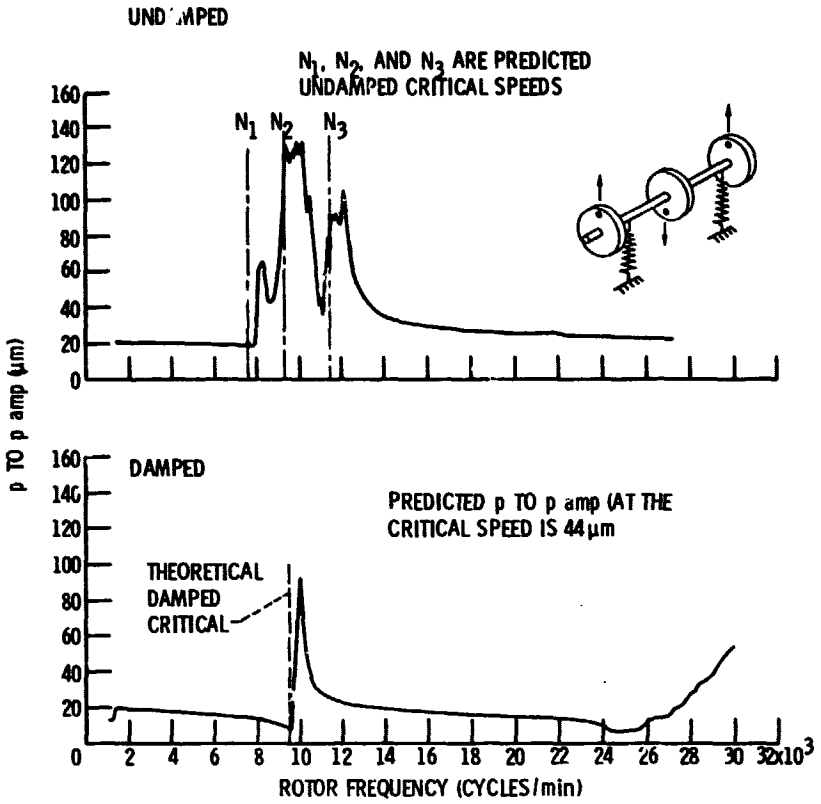

Figure 7. - Comparison of rotor response for undamped and damped conditions type I unbalanced distribution; U = 0.93 gm-cm; no. 3 disk.

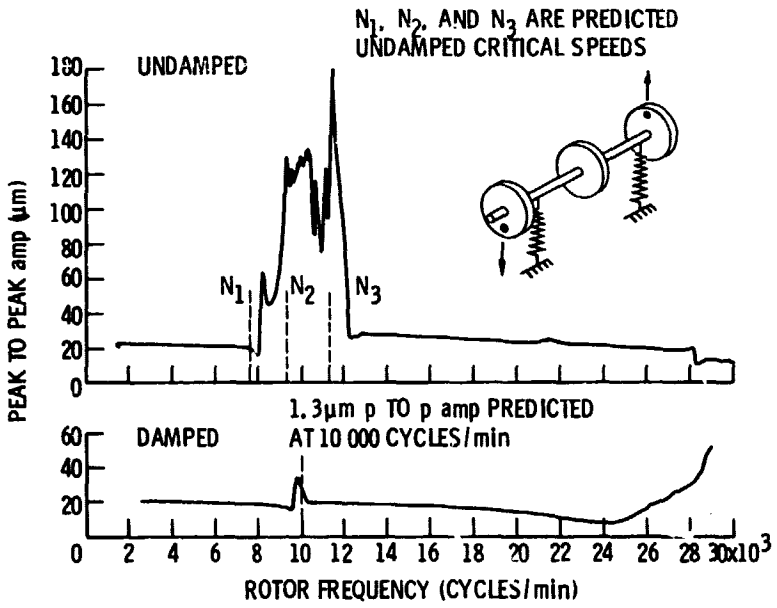

Figure 8. - Comparison of rotor response for undamped versus damped conditions N = 3 disk. Type II unbalanced distribution; U = 0.62 gm-cm.

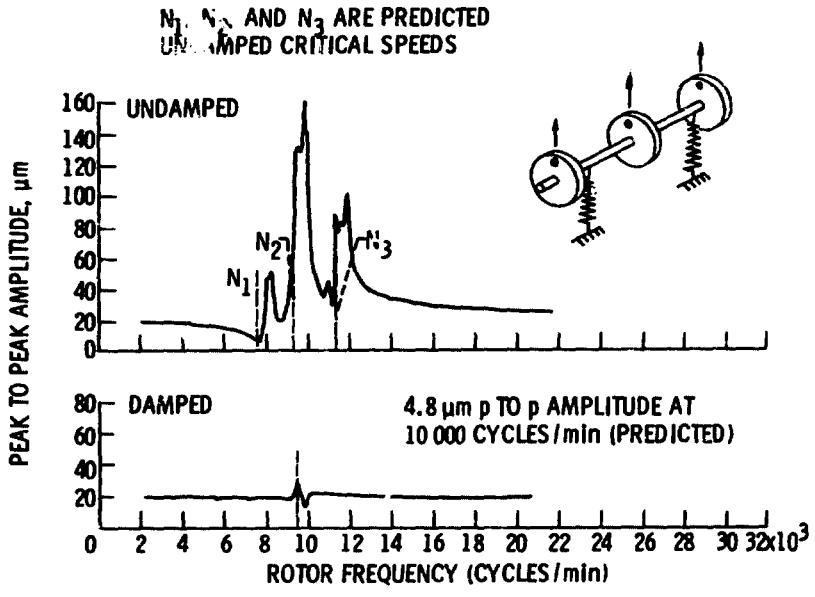

Figure 9. - Comparison of rotor response for undamped and damped conditions, no. 3 disk, type III unbalanced distribution U = 0.93 gm-cm.

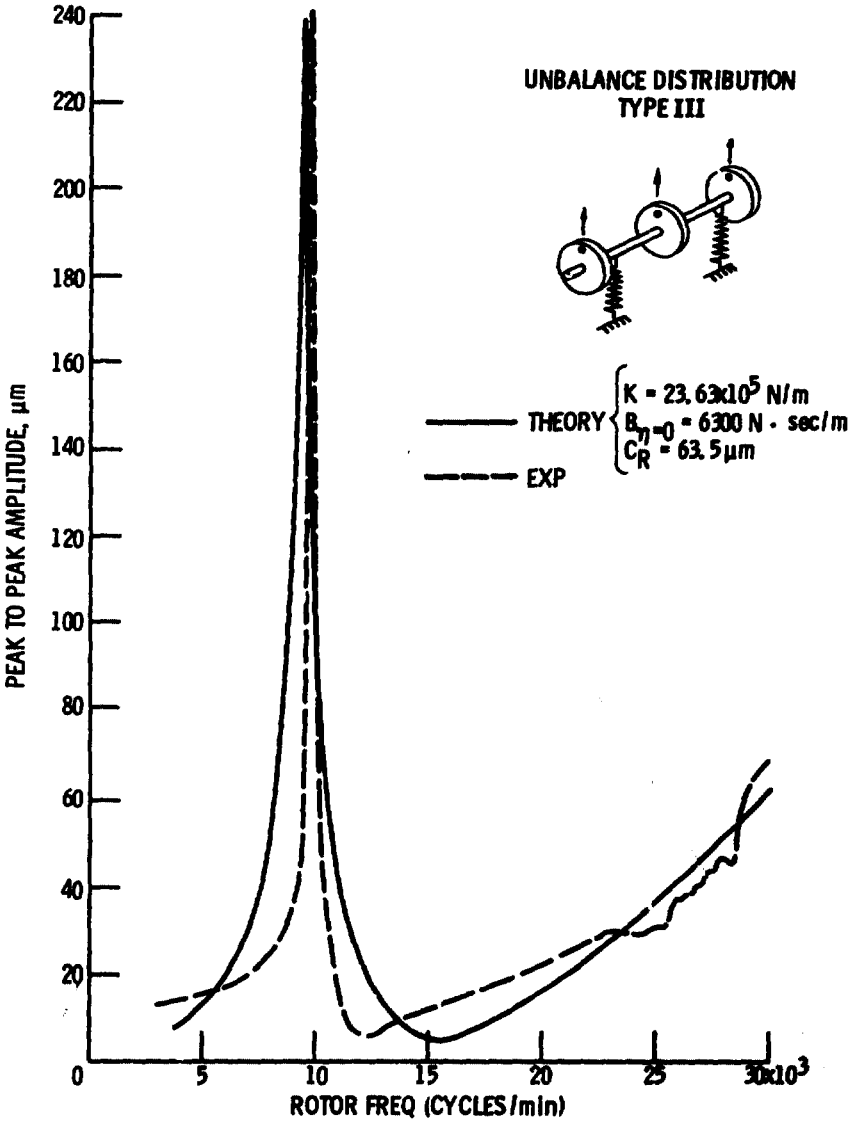

(a) CENTER DISK.

Figure 10. - Comparison of experimental with theoretical damped rotor response, total unbalance = 10.6 gm-cm.

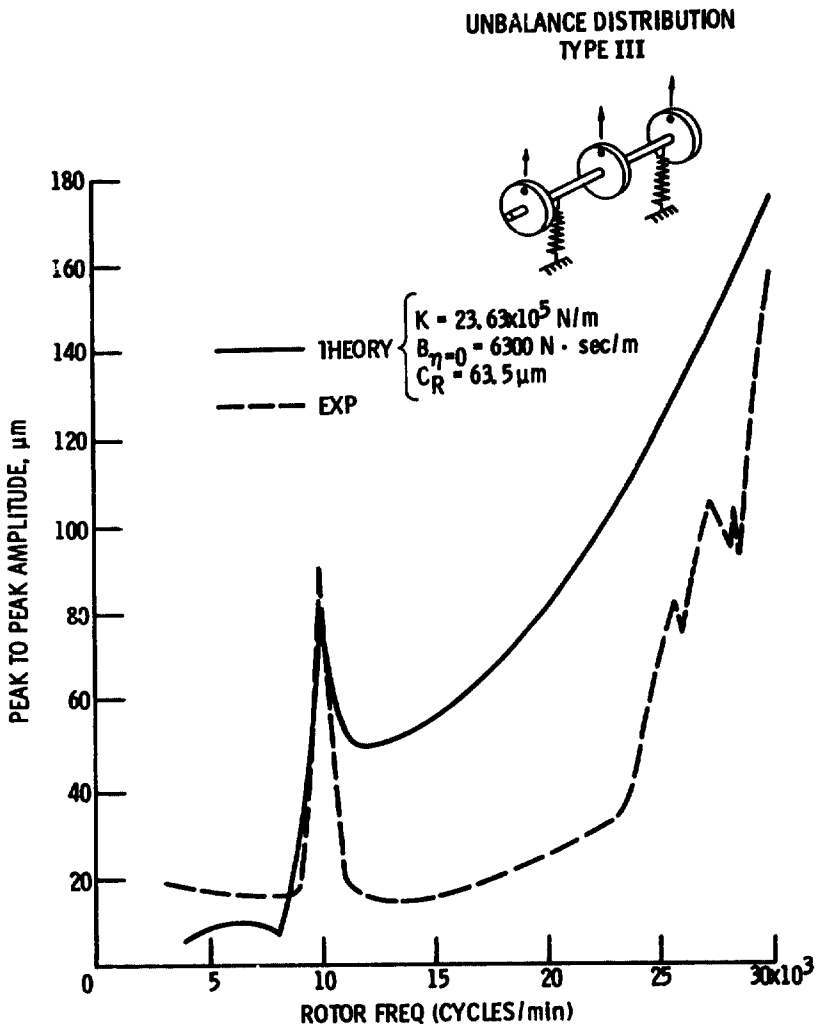

(b) NO. 3 DISK.

Figure 10. - Continued.

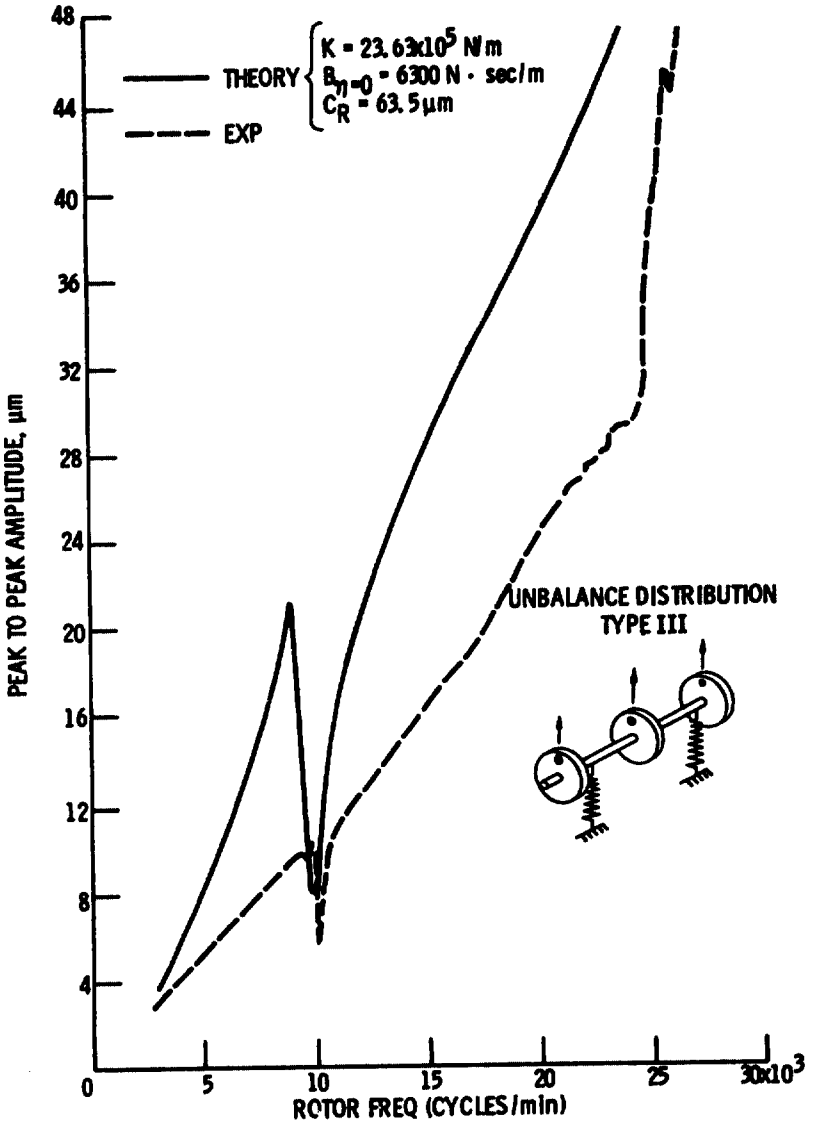

(c) DAMPER JOURNAL, NO. 2 BEARING.

Figure 10. - Continued.

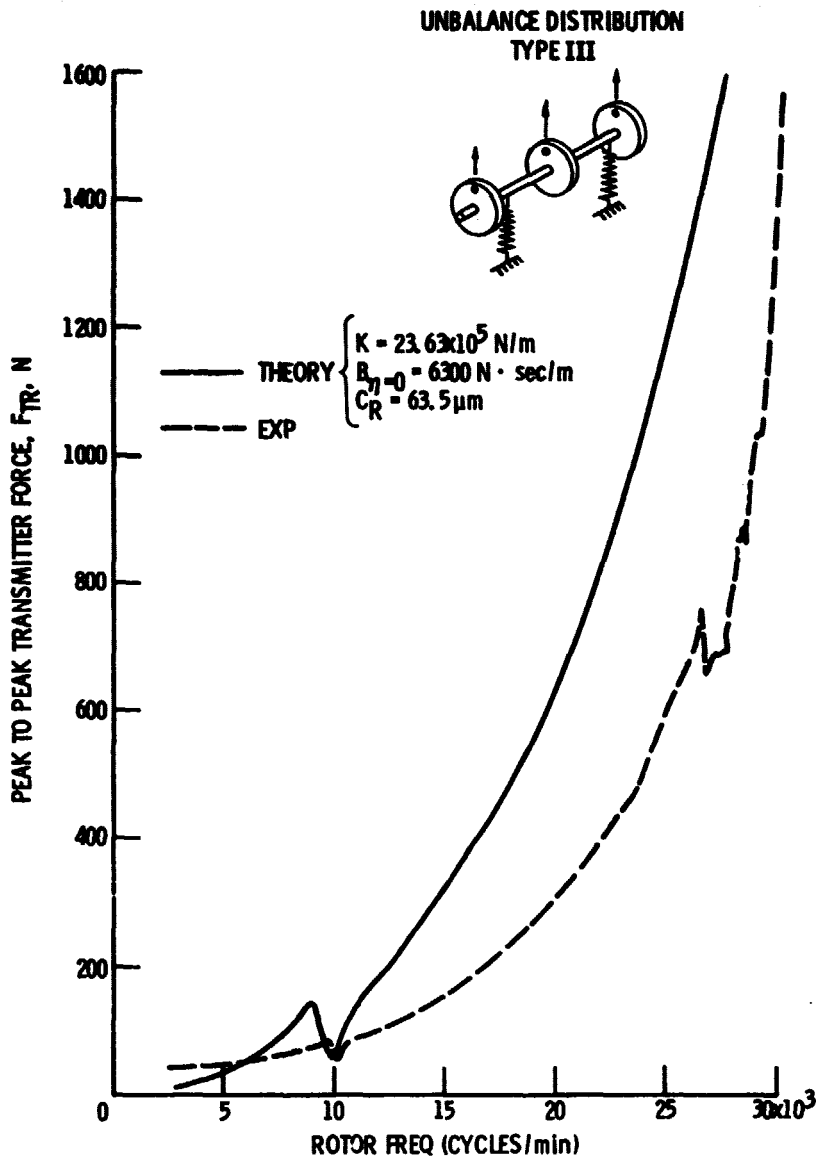

(d) TRANSMITTED FORCE AT NO. 2 BEARING.

Figure 10. - Concluded.

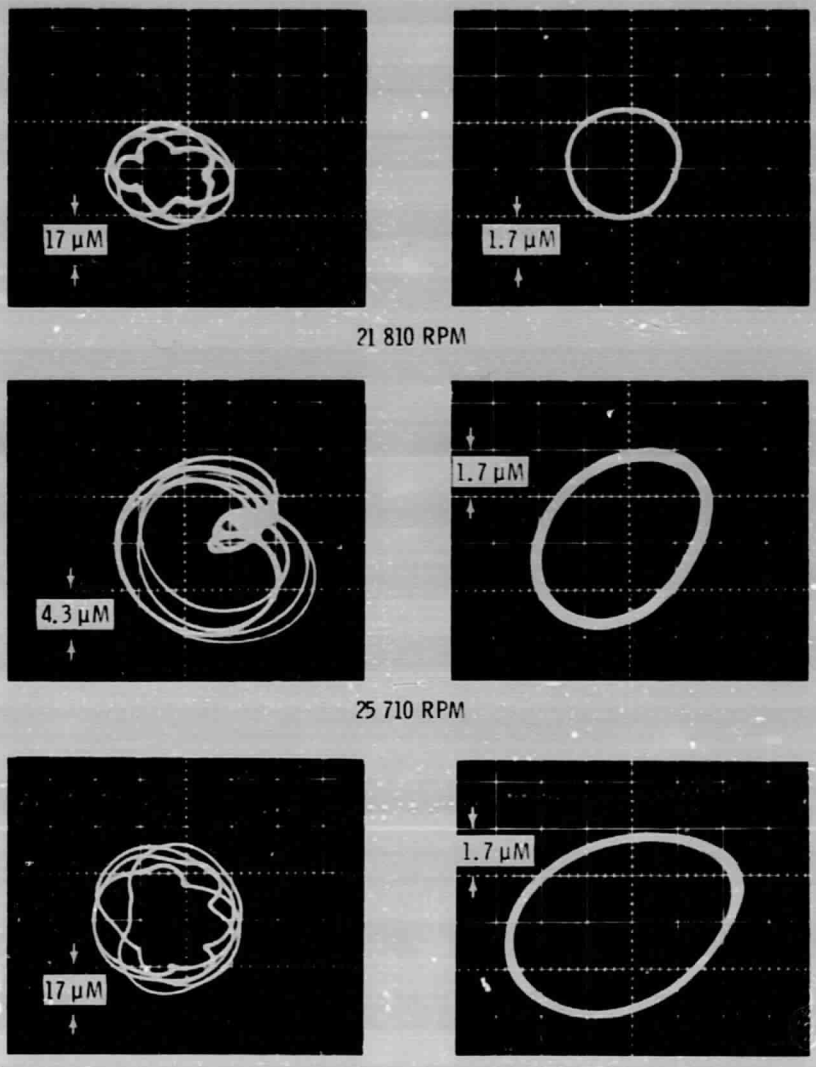

Figure 11(a). - Orbital motion of damper journal (BRG No. 2) with and without oil. Clearance, C = 63.5 μM; oil flow, 5.15×10^{-4} m^3/min; supply pressure, 19.29×10^4 N/M^2; unbalance distribution type I, U = 0.93 GM-CM.

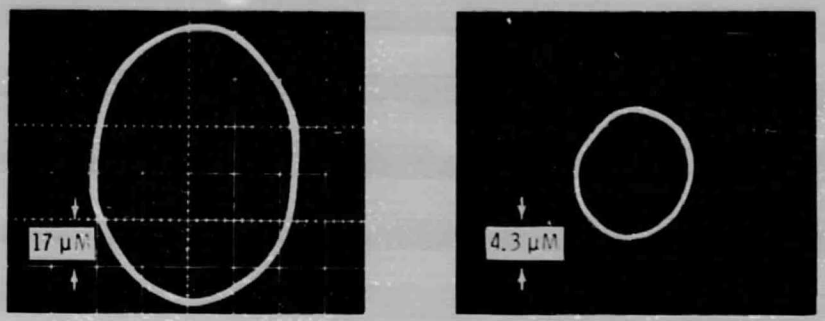

9020 RPM 9030 RPM

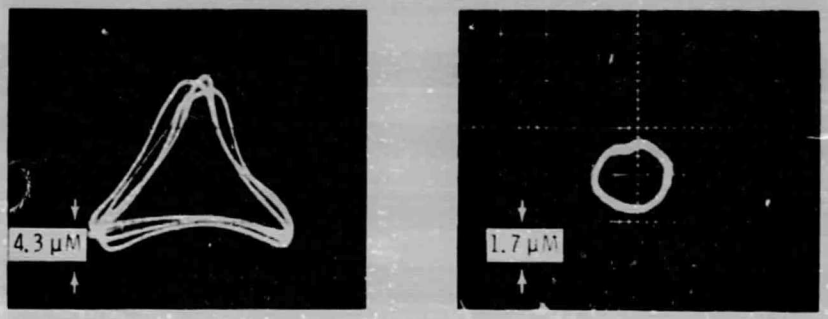

14 820 RPM

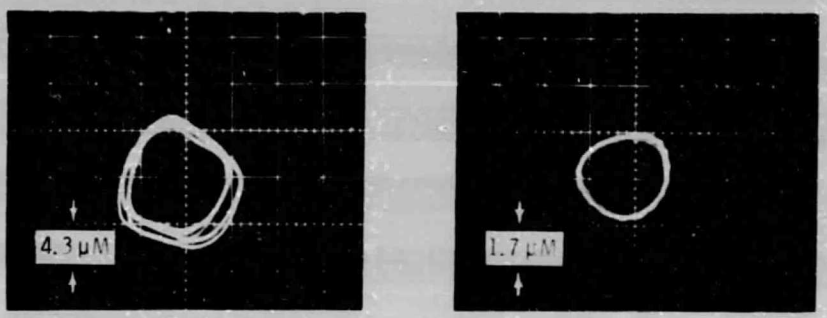

29 500 RPM

UNDAMPED RESPONSE DAMPED RESPONSE

Figure 11(a). - Concluded. Orbital motion of damper journal BRG No. 2 with and without oil. Clearance, C = 63.5 μM; oil flow, 5.15×10^{-4} m^3/min; supply pressure, 19.29×10^4 N/M^2; unbalance distribution type I; U = 0.93 GM-CM.

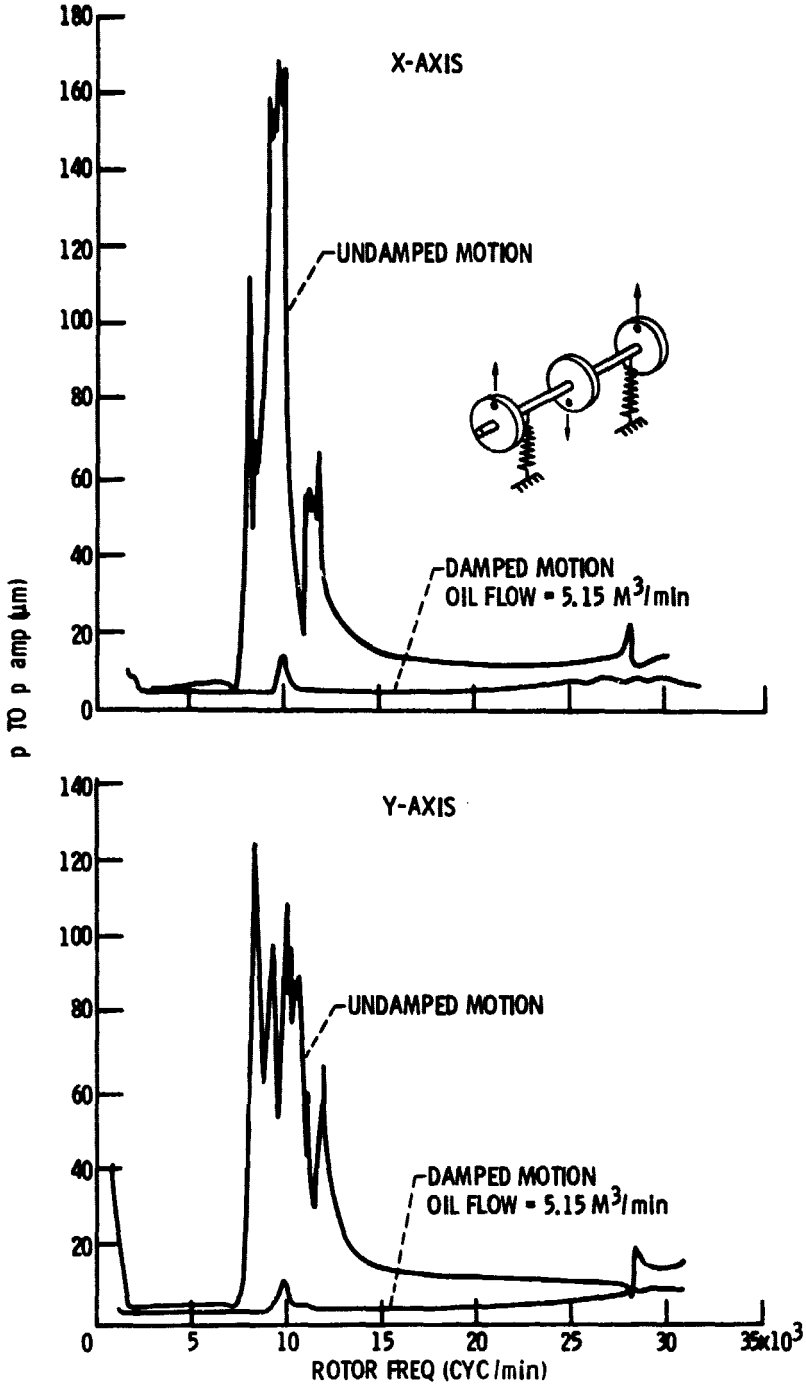

Figure 11(b). - Comparison of damper journal motion at bearing no. 2 with and without squeeze film damping. Type I unbalance distribution. $U = 0.93$ gm-cm; $C_R = 63.5$ µm.

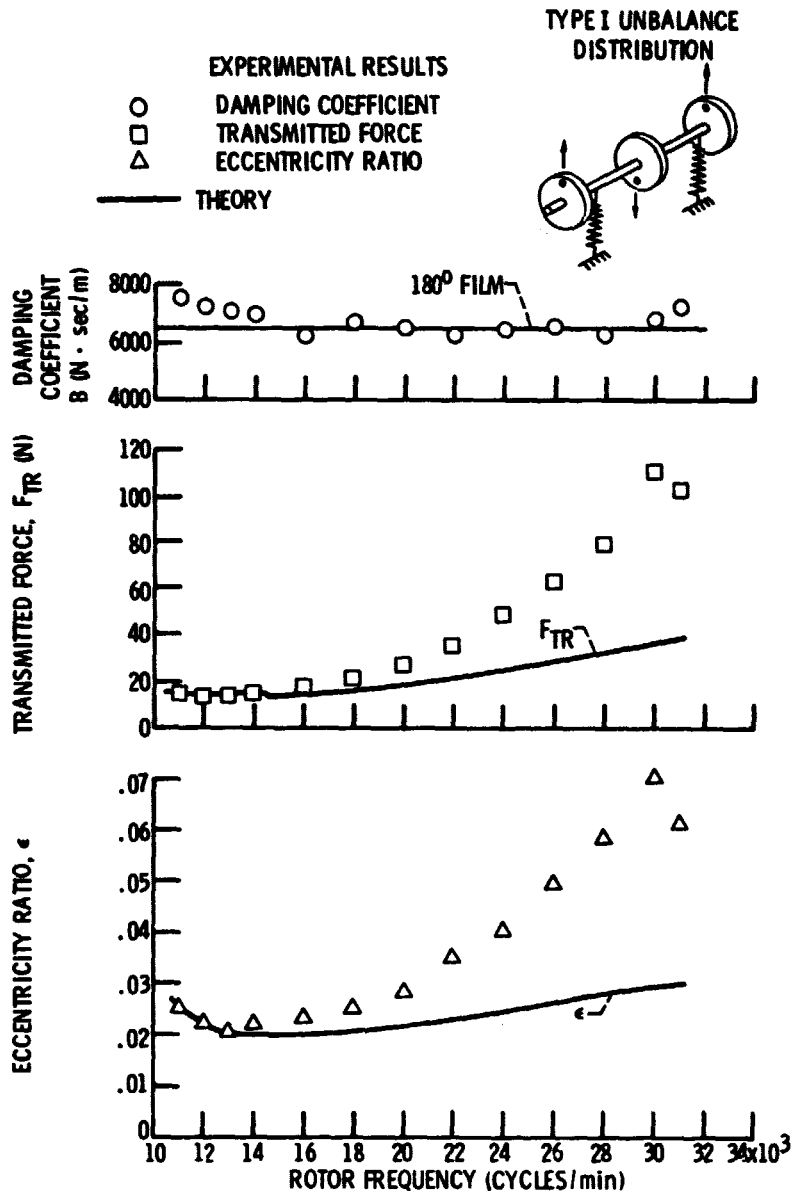

(a) U = 0.93 gm-cm.

Figure 12. - Comparison between theory and experiment of damping coefficients, transmitted forces and eccentricity ratios as functions of rotor frequency.

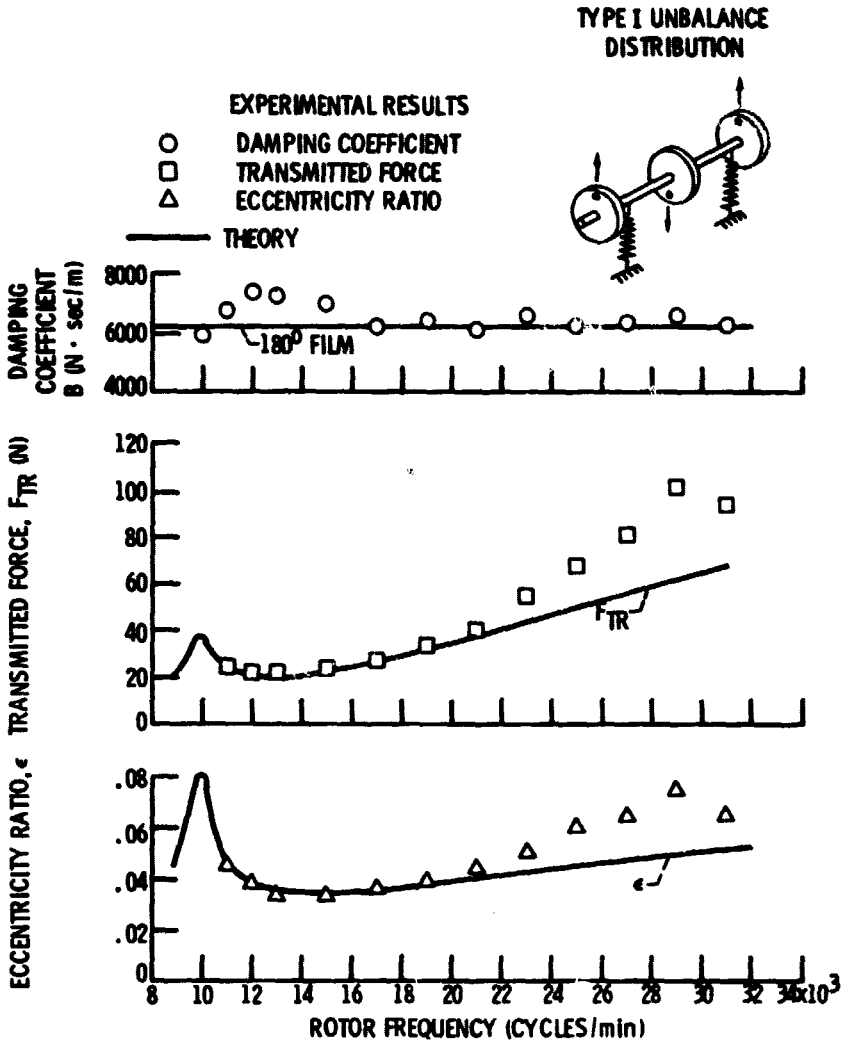

(b) U = 1.67 gm-cm.

Figure 12. - Concluded.

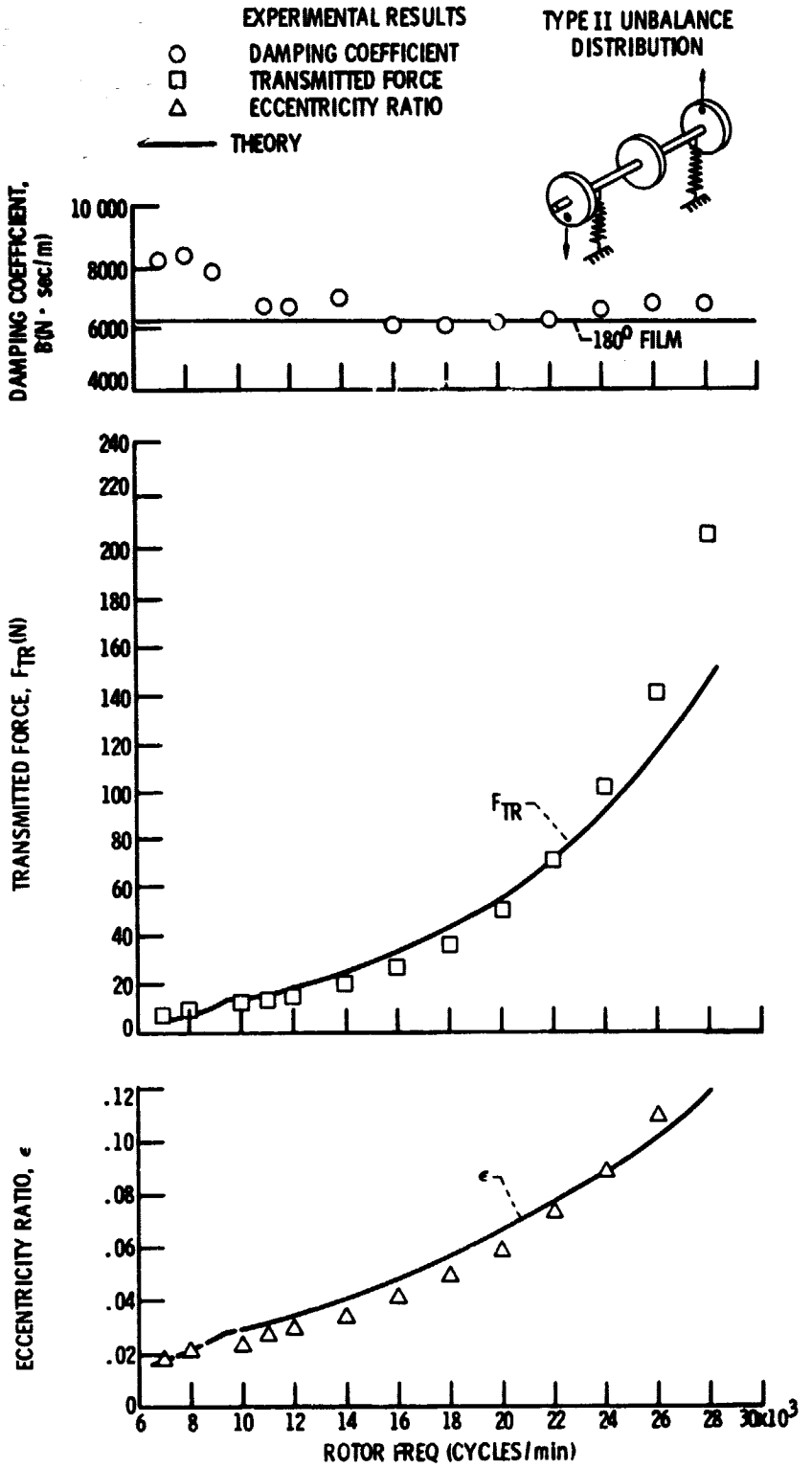

(a) U = 1.5 gm-cm.

Figure 13. - Comparison between theory and experiment of damping coefficients, transmitted forces and eccentricity ratios as functions of rotor frequency.

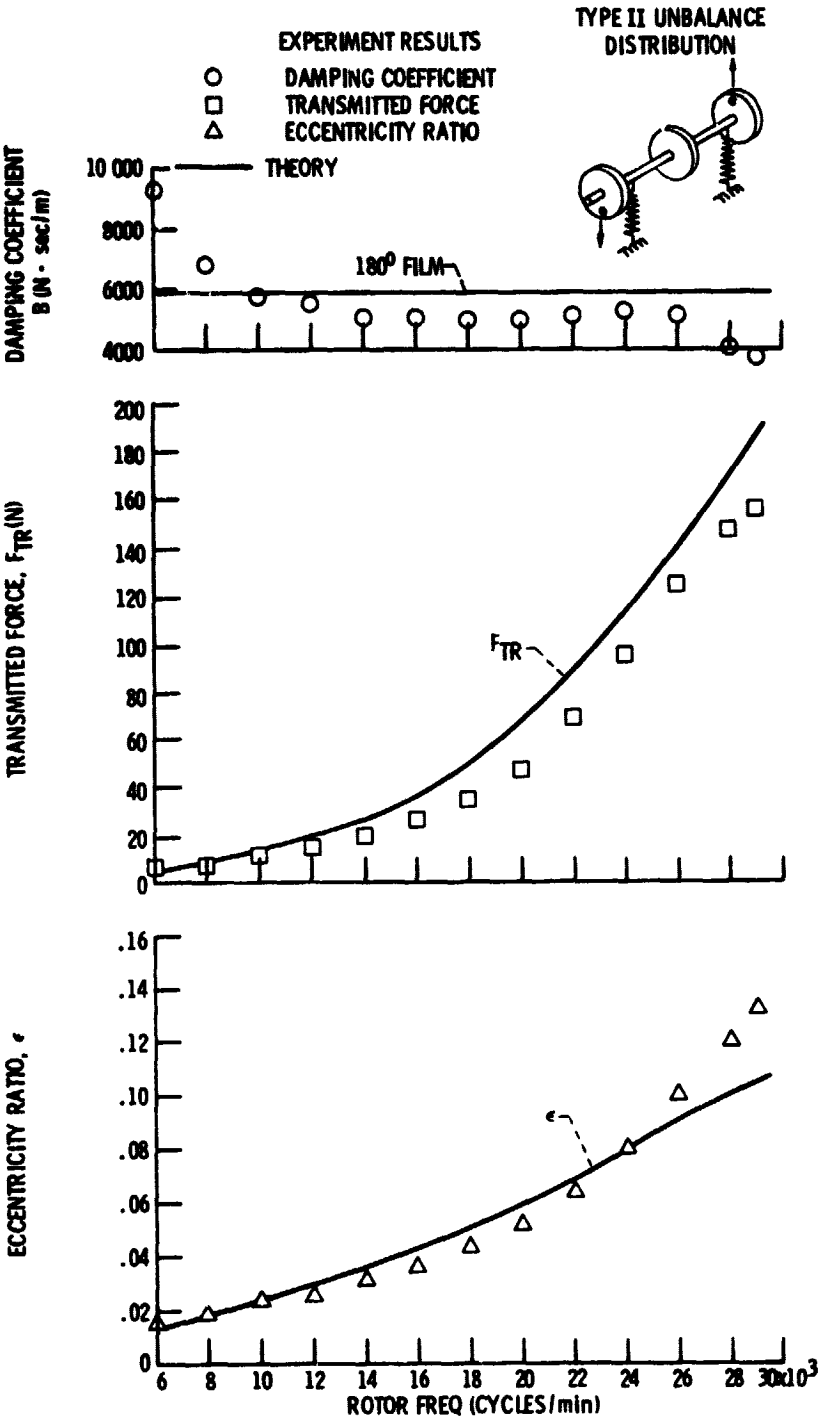

(b) U = 3.3 gm-cm.

Figure 13. - Concluded.

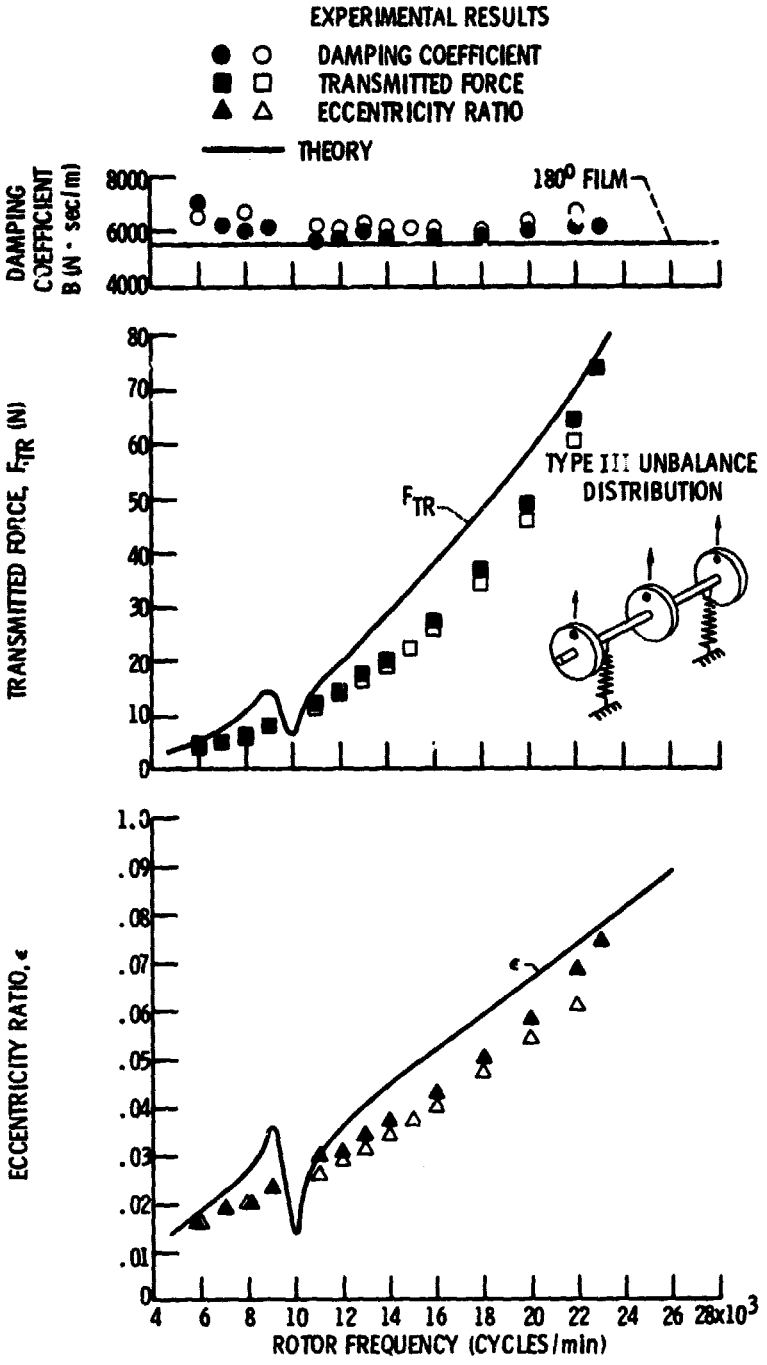

(a) U = 2.25 gm-cm.

Figure 14. - Comparison between experiment and theory of damping coefficients, transmitted forces and eccentricity ratios as functions of rotor frequency.

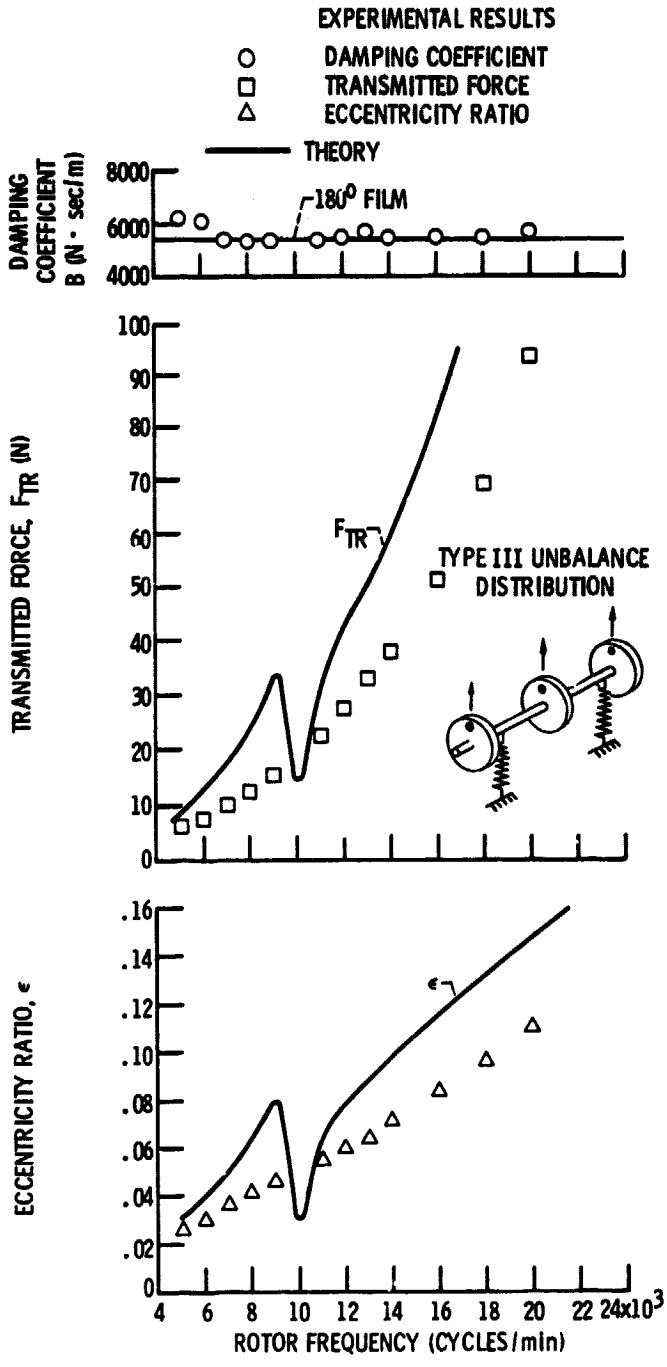

(b) U = 4.97 gm-cm.

Figure 14. - Continued.

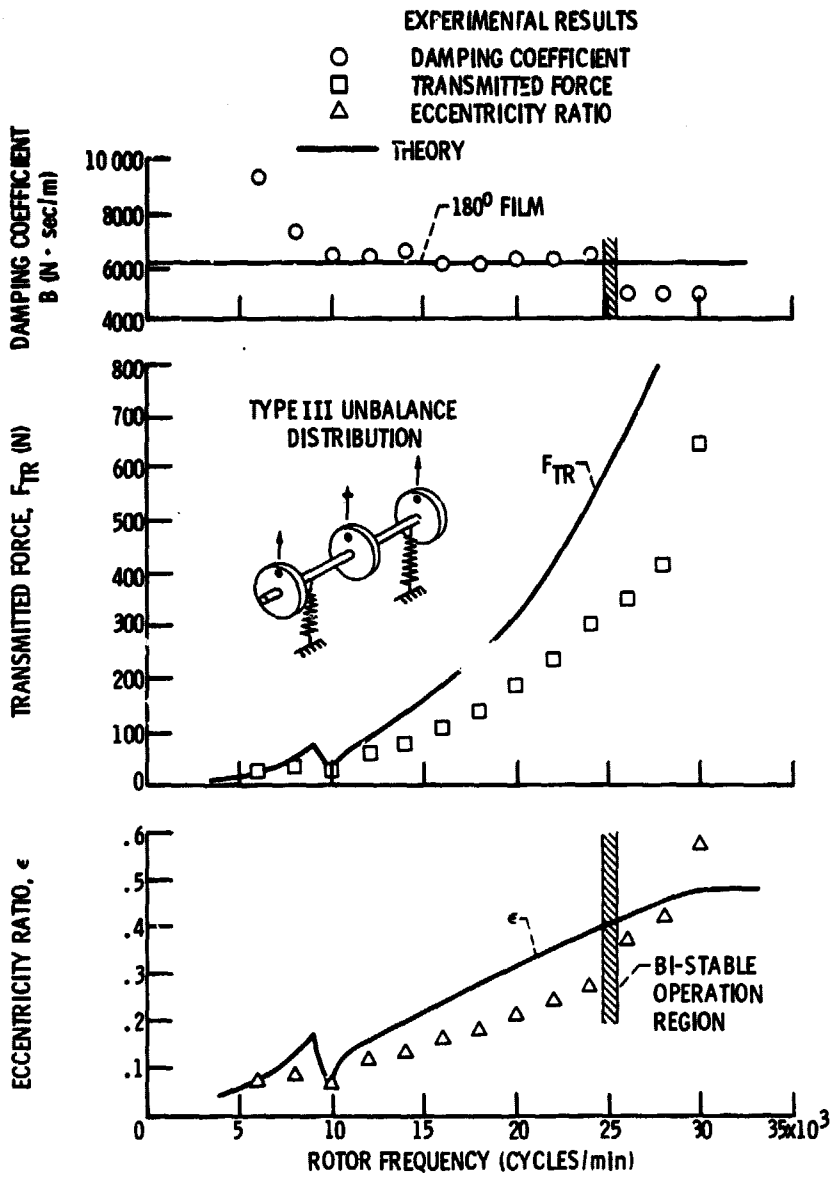

(c) U = 10.6 gm-cm.

Figure 14. - Continued.

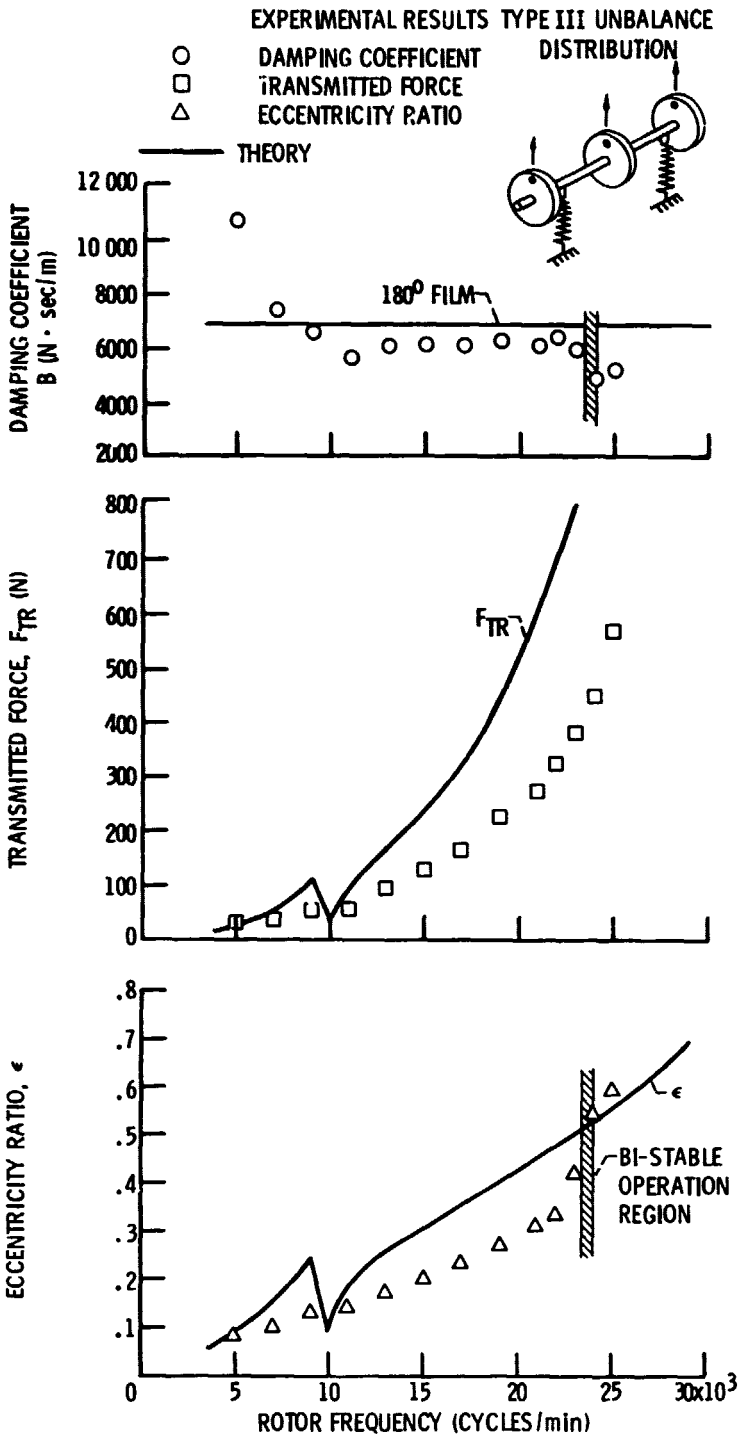

(d) U = 15.1 gm-cm.

Figure 14. - Concludad.